SUPPORTING INFORMATION

Solvent-controlled solid-state phase transitions of heterospin Cu(II) complex with imidazolyl-substituted nitronyl nitroxide

Kristina A. Smirnova, Irina V. Golomolzina, Galina V. Romanenko, Sergey V. Fokin, Svyatoslav E. Tolstikov, Gleb A. Letyagin, Platon A. Chernavin, Artem S. Bogomyakov*

International Tomography Center, 3a Institutskaya St., Novosibirsk 630090, Russia

**Corresponding author*

E-mail: bus@tomo.nsc.ru

Content

1. Crystal data

Table S1. Crystallographic characteristics of the studied compounds and experimental details **1**$_2$, **1**, **1**·0.5CH_2Cl_2, **1**·0.5CH_2Br_2, **1**·0.5$CHCl_3$

	1$_2$	**1**	**1**·0.5Solv				
Solv	–	–	CH_2Cl_2	CH_2Br_2	$CHCl_3$		
Color	violet	greenish-brown	green	green	green		
	Binuclear	Chain	Chain	Chain	Chain		
FW	1485.98	742.99	785.46	829.92	802.68		
T, K	296	296	296	296	296	250	100
Space group, *Z*	$P2_1/c$, 2	$P2_1/n$, 4	*Fdd*2, 16	*Fdd*2, 16	*Fdd*2, 16		
a, *b*, *c*, Å	11.3929(3) 17.1560(5) 15.8310(4)	12.4968(4) 21.3202(6) 13.1871(3)	22.7207(4) 45.4461(7) 12.8963(2)	22.7627(7) 45.5849(12) 12.9118(4)	22.8425(9) 45.5319(16) 12.9843(5)	22.709(3) 45.424(6) 12.9488(16)	22.6386(6) 45.1154(13) 12.6581(3)
β, °	90.643(2)	116.5985(17)	90	90	90	90	90
V, Å^3	3094.08(14)	3141.65(16)	13316.3(4)	13397.7(7)	13504.5(9)	13357(3)	12928.3(6)
D_c, g cm^{-3}	1.595	1.571	1.567	1.646	1.579	1.596	1.650
ϑ_{max}, deg.	28.364	67.935	67.999	28.292	28.709	29.173	28.763
I_{hkl} (meas/uniq), R_{int}	28439 / 7709 0.0544	225872 / 5612 0.0839	46671 / 6024 0.0366	37880 / 8219 0.0592	34360 / 8342 0.0589	33394 / 8409 0.0724	30065 / 7908 0.0737
I_{hkl} (I>2σ_I) / Ns	3379 / 523	3372 / 496	5790 /	3489 / 465	3791 / 478	3869 / 478	3830 / 480
GooF	0.964	0.859	1.067	0.824	0.777	0.794	0.873
R_1 / wR_2 (I>2σ_I)	0.0518 / 0.1155	0.0429 / 0.1067	0.0384 / 0.1052	0.0487 / 0.1079	0.0419 / 0.0833	0.0427 / 0.0773	0.0537 / 0.1117
CCDC	2350246	2350245	2350255	2350253	2350252	2350251	2350250

Table S2. Crystallographic characteristics of the studied compounds and experimental details **1**·0.5Solv (Solv = $(CH_3)_2CO$, THF)

Solv	$(CH_3)_2CO$			THF		
T, K	296	200	100	296	200	150
Color	green	green	green	green	green	green
FW	772.03	772.03	772.03	779.04	779.04	779.04
Space group, *Z*	*Fdd*2, 16	*Fdd*2, 16	*Cc*, 24	*Fdd*2, 16	*Fdd*2, 16	*Fdd*2, 16
a, *b*, *c*, Å	22.8017(19) 45.614(4) 12.8802(10)	22.5627(15) 45.487(3) 12.7439(8)	12.6230(6) 45.631(2) 33.8261(16)	22.8465(15) 45.601(3) 12.9362(8)	22.625(4) 45.441(7) 12.789(2)	22.9206(10) 45.728(2) 12.1832(6)
β, °	90	90	100.590(3)	90	90	90
V, Å^3	13396(2)	13079(1)	19152.0(16)	13477.3(15)	13149(4)	12769.5(10)
D_c, g cm^{-3}	1.531	1.568	1.607	1.536	1.574	1.621
ϑ_{max}, deg.	28.323	28.108	28.720	67.854	28.299	28.794
I_{hkl} (meas/uniq) R_{int}	38553 / 8329 0.0874	37070 / 7943 0.0570	85767 / 30302 0.0896	15750 / 5350 0.1014	28221 / 8061 0.1136	29755 / 8011 0.1061
I_{hkl} ($I>2\sigma_I$) / Ns	3175 / 460	4459 / 479	21807 / 2601	3989 / 436	3771 / 560	3392 / 490
GooF	0.997	0.914	0.884	1.006	0.936	0.973
R_1 / wR_2 ($I>2\sigma_I$)	0.0355 / 0.04492	0.0411 / 0.0825	0.0582 / 0.1044	0.743 / 0.1958	0.0582 / 0.1066	0.0585 / 0.0804
CCDC	2350254	2350249	2350256	2350244	2350248	2350247

3. Crystal packing

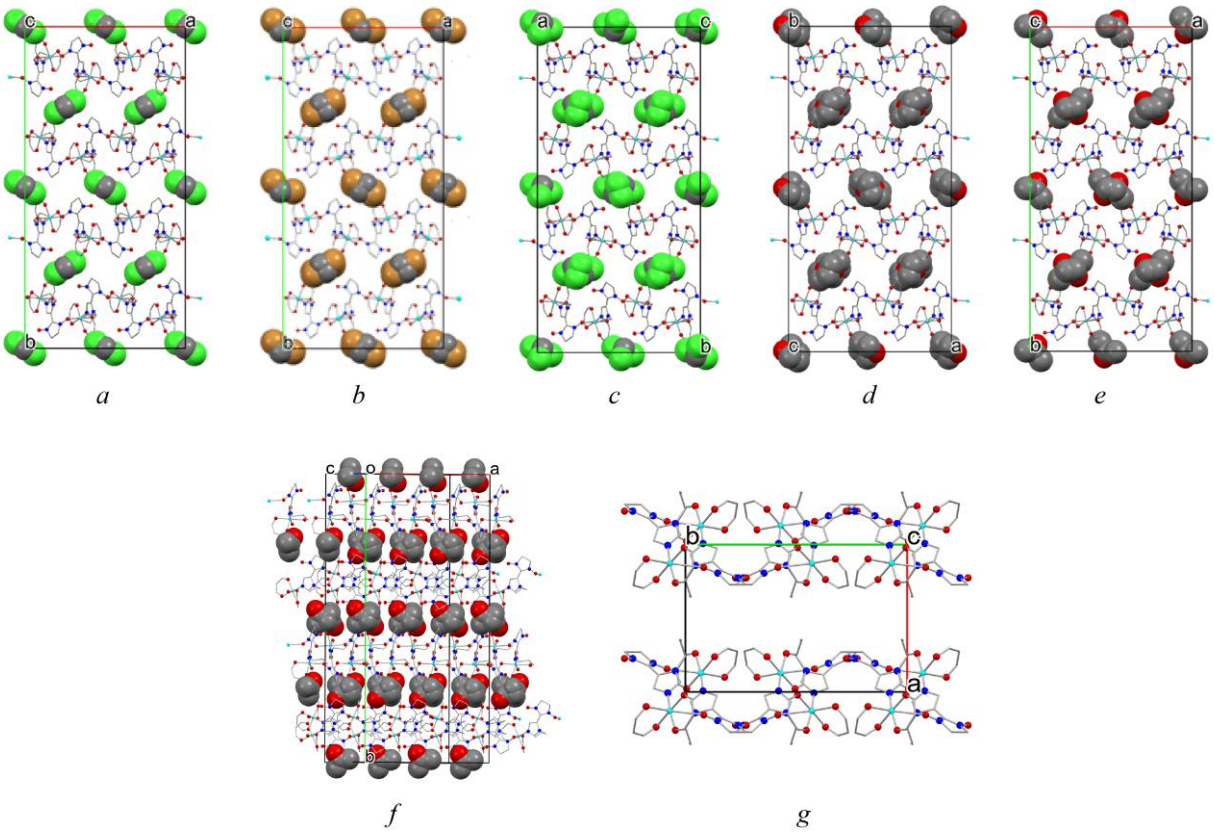

Figure S1. Crystal packing along the *c*-axis of complexes **1**·0.5Solv, Solv = CH_2Cl_2 (*a*), CH_2Br_2 (*b*), $CHCl_3$ (*c*), THF (*d*), $(CH_3)_2CO$ (*e*); crystal packings of **1**·0.5$(CH_3)_2CO$ (*f*) and $\mathbf{1_2}$ (*g*), viewed from a specific orientation, reveal that a repeating pattern within half of the chains in 1·0.5$(CH_3)_2CO$ closely resembles the arrangement of the binuclear molecules in $\mathbf{1_2}$. The solvent molecules are shown in space-filling mode.

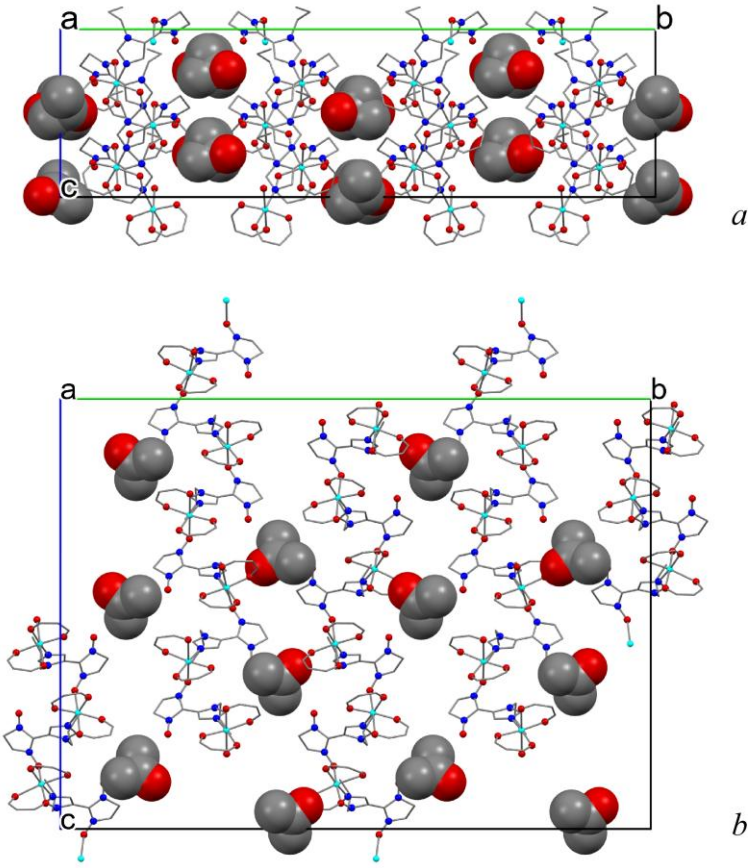

Figure S2. Crystal packing of **1**·0.5$(CH_3)_2CO$ before (*a*, at 296 K) and after phase transition (*b,* at 100 K) along *c* axis; Solvent molecules are shown in space-filling mode.

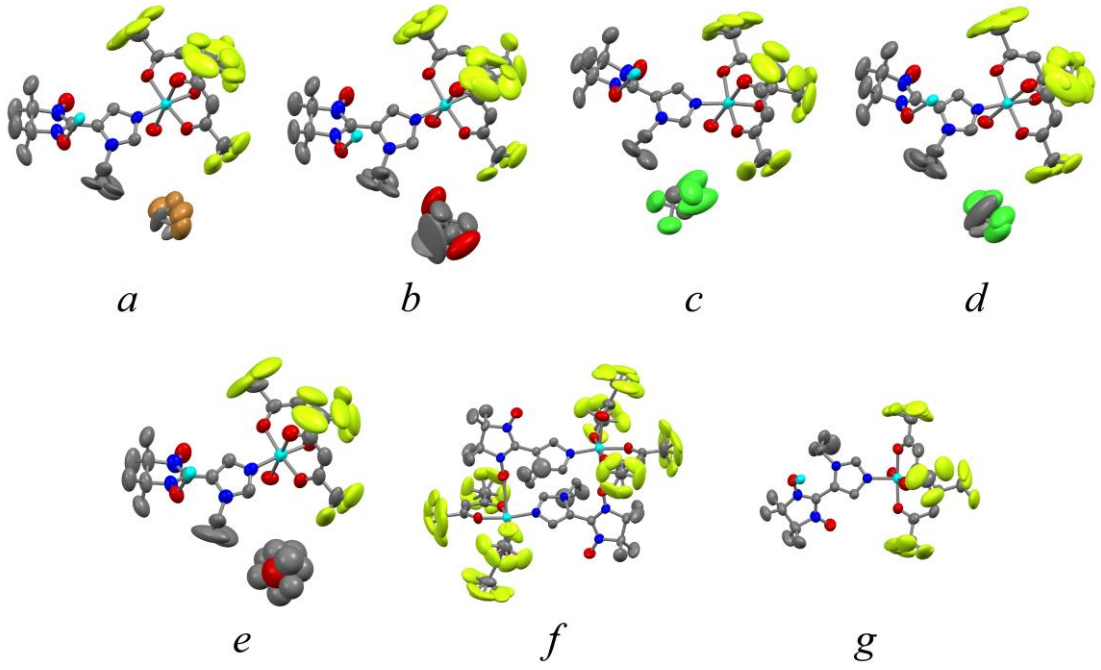

Figure S3. Chain structures of **1**·0.5Solv, Solv = CH_2Br_2 (*a*), $(CH_3)_2CO$ (*b*), CH_2Cl_2 (*c*), $CHCl_3$ (*d*), THF (*e*), **1** (*f*), and $\mathbf{1}_2$ (*g*) at 296 K with thermal ellipsoids at a 50% probability level.

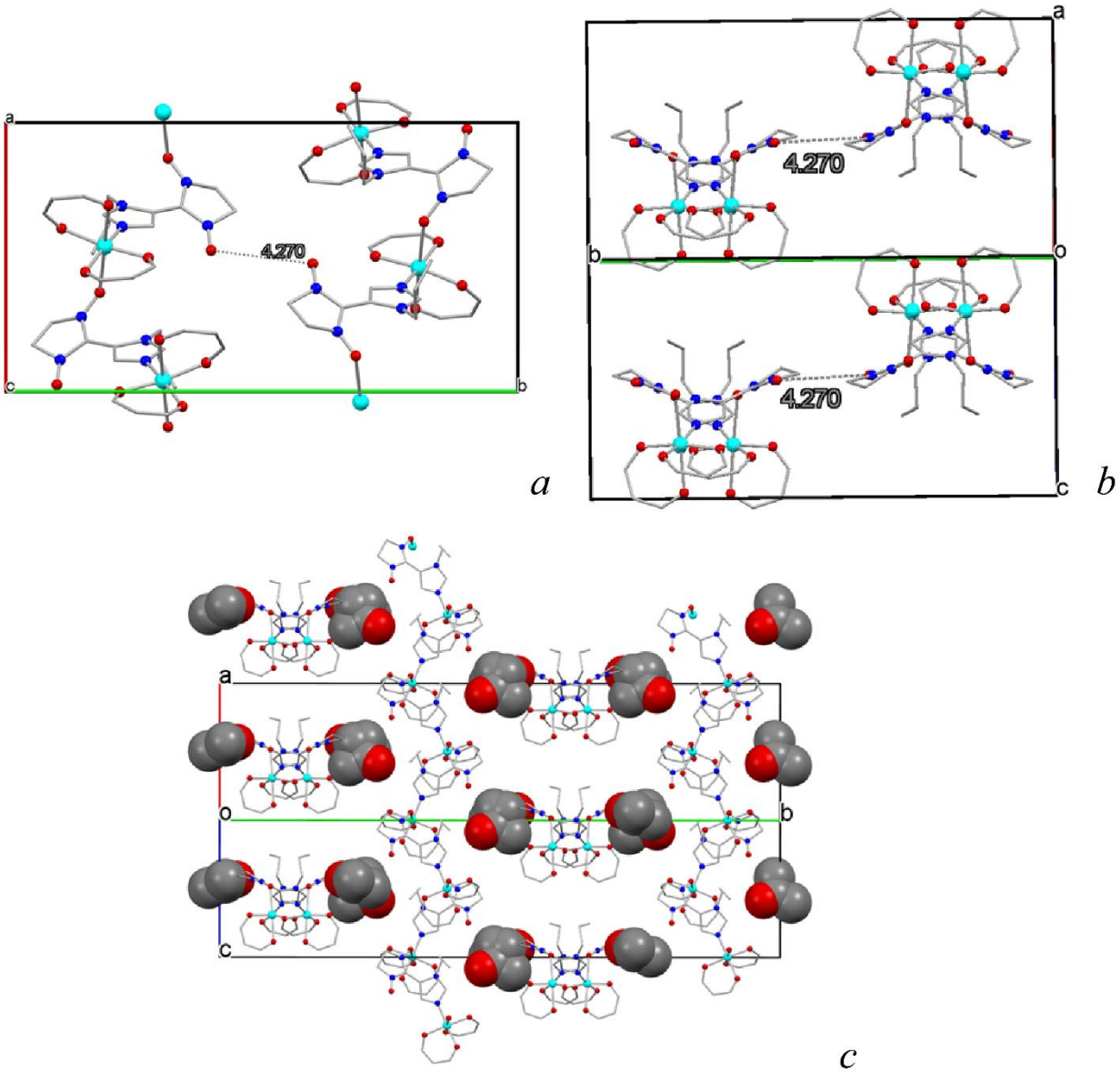

Figure S4. Crystal packing of **1** (*a*, *b*) and **1**·0.5$(CH_3)_2CO$ (*c*).

4. Magnetic field dependences of magnetization

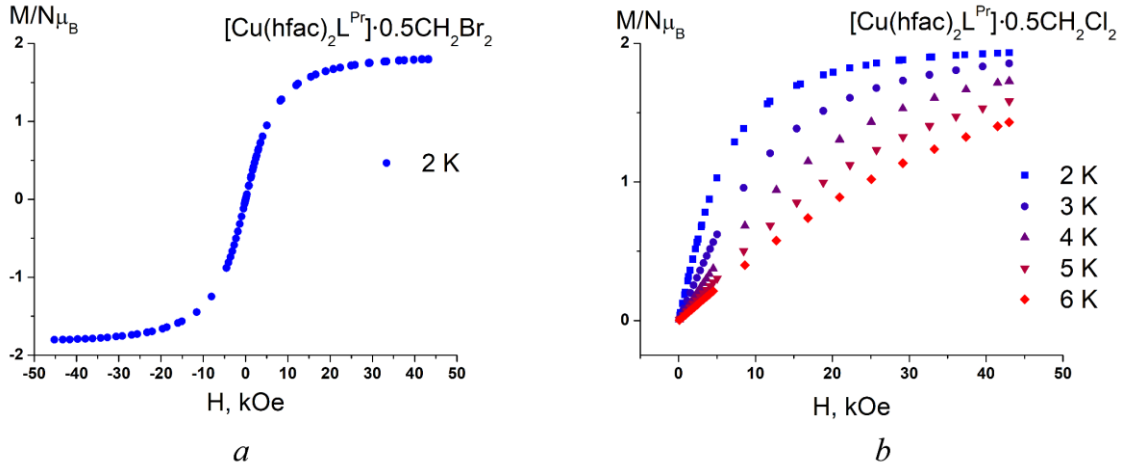

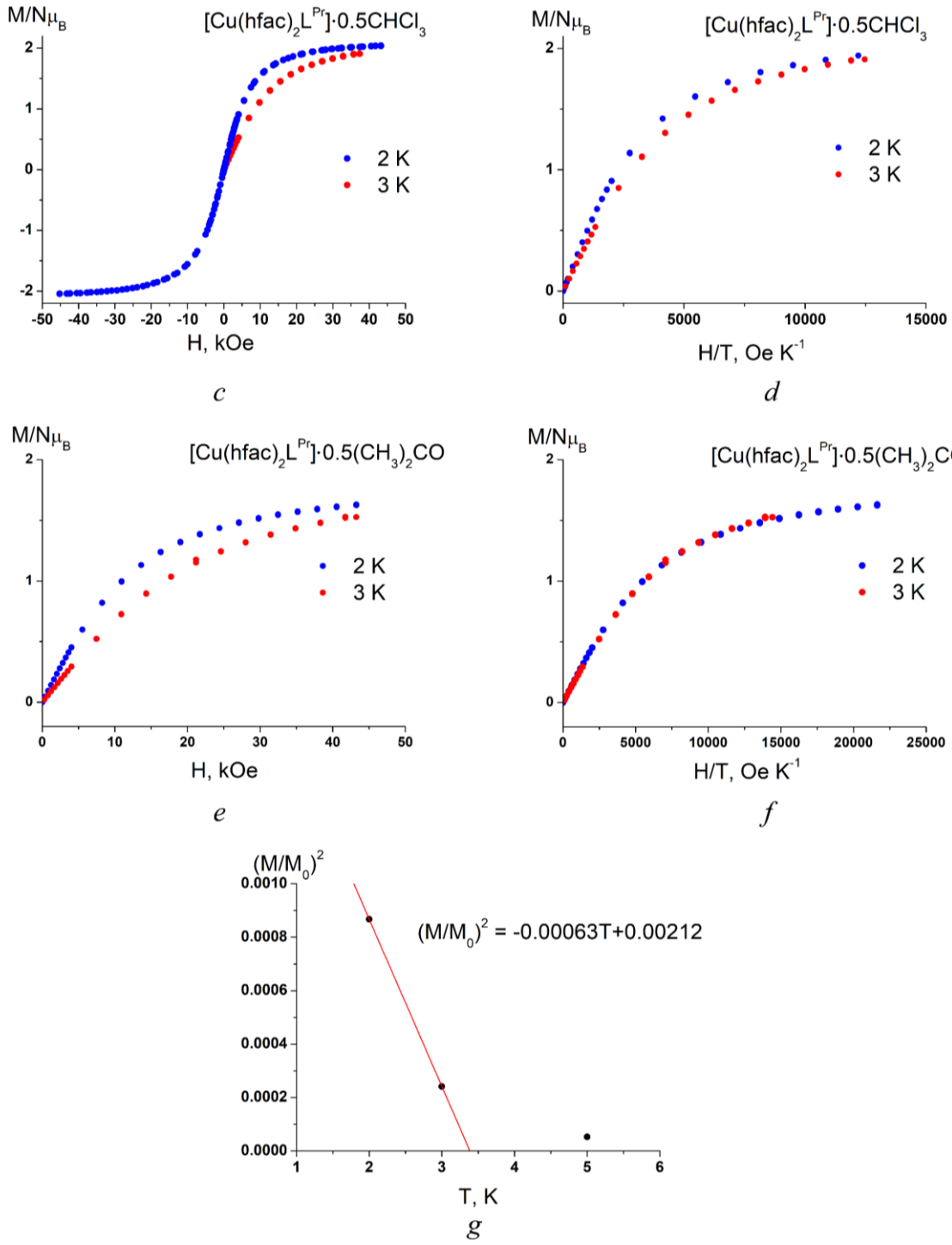

Figure S5. Field-dependences of magnetization M(H) for **1**·0.5Solv, Solv = CH_2Br_2 (*a*), CH_2Cl_2 (*b*), $CHCl_3$ (*c*), $(CH_3)_2CO$ (*e*); M(H/T) curves for **1**·0.5Solv, Solv = $CHCl_3$ (*d*), $(CH_3)_2CO$ (*f*). Illustration of determination of Curie temperature T_C ~3.3 K from the dependence $(M/M_0)^2(T)$, where $M_0 = gSN\mu_B = 2N\mu_B$ – saturation magnetization, the value of the magnetization M is determined at H = 250 Oe (*g*).

5. Changes in the single crystal diffraction patterns during the chain-to-dimer transformation

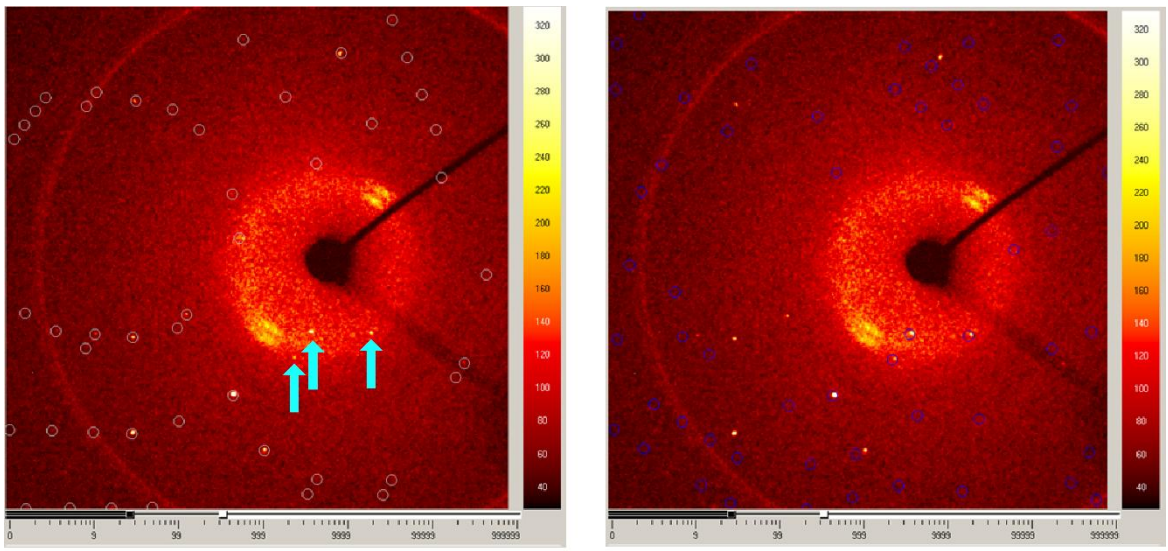

a *b*

Figure S6. Single crystal X-ray diffraction patterns of **1**·0.5$(CH_3)_2CO$ freshly prepared single crystal: circles indicate the reflections of the orthorhombic **1**·0.5$(CH_3)_2CO$ (*a*) and monoclinic $\mathbf{1}_2$ (*b*) at 6 hours after the start of the experiment. The blue arrows point at the reflections of $\mathbf{1}_2$ that obviously cannot be attributed to the reflections of **1**·0.5$(CH_3)_2CO$.

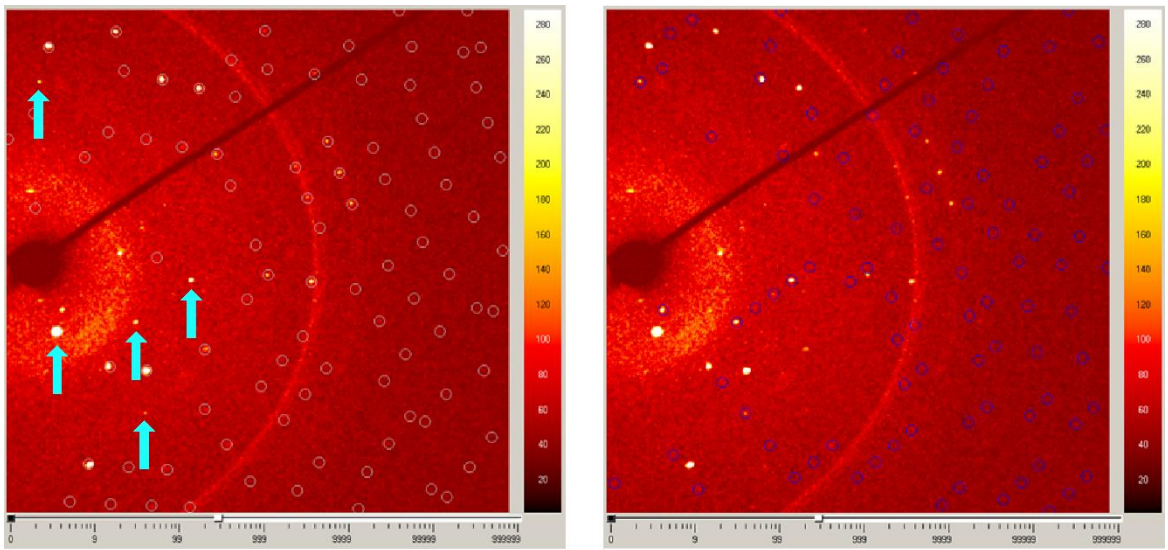

a *b*

Figure S7. Single crystal X-ray diffraction patterns of **1**·0.5CH_2Cl_2 single crystal derived from a desiccator: circles indicate the reflections of the orthorhombic **1**·0.5CH_2Cl_2 (*a*) and monoclinic $\mathbf{1}_2$ (*b*). The blue arrows point at the reflections of $\mathbf{1}_2$ that obviously cannot be attributed to the reflections of **1**·0.5CH_2Cl_2.

6. Changes in color of single crystals and polycrystalline samples

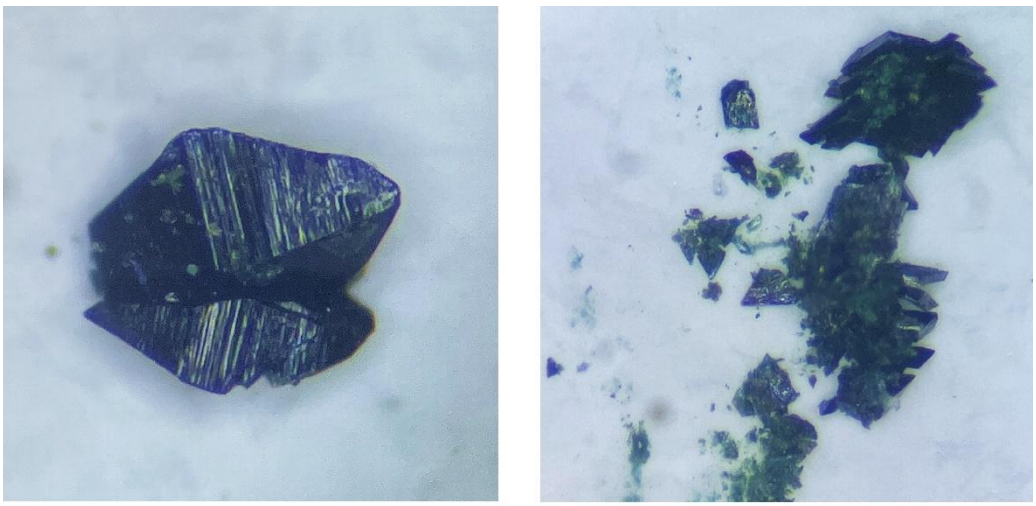

a *b*

Figure S8. Crystals of **1**·0.5CH_2Br_2, left in the open air for several days (*a*), the same crystals, but fractured (*b*). The surface turned violet, but inside they remained green.

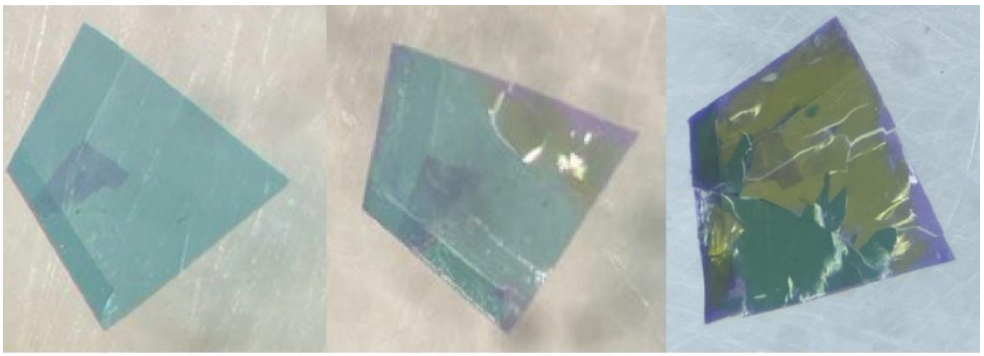

a *b* *c*

Figure S9. Thin plate crystal of freshly prepared **1**·0.5CH_2Br_2 (*a*), the crystal on the following day (*b*), and under different lighting two days later (*c*). The purple, green-brown, and green colors correspond to $\mathbf{1}_2$, **1** and **1**·0.5$(CH_3)_2CO$, respectively.

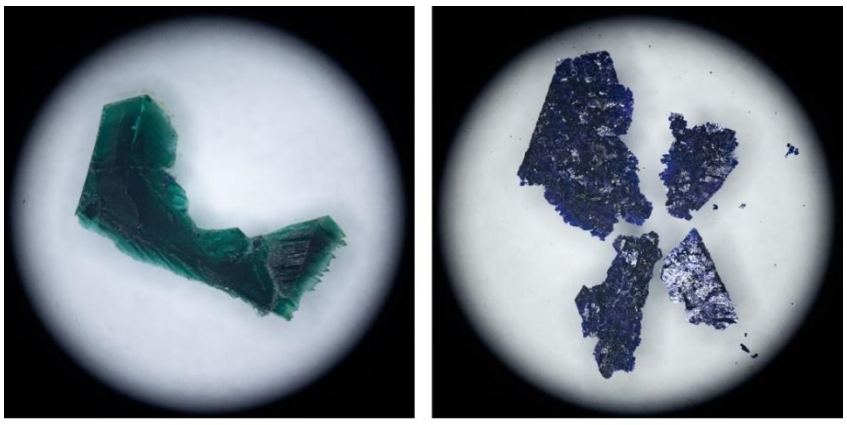

a *b*

Figure S10. Crystals of **1**·0.5$(CH_3)_2CO$ (*a*) and the same crystals, but after being kept under a layer of *n*-heptane for a day (*b*). The color of the crystals changed from green to violet, and their diffraction pattern now fully corresponds to the single crystal of $\mathbf{1}_2$, which confirms the single-crystal-to-single-crystal transformation of solvates to $\mathbf{1}_2$ under a layer of *n*-heptane.

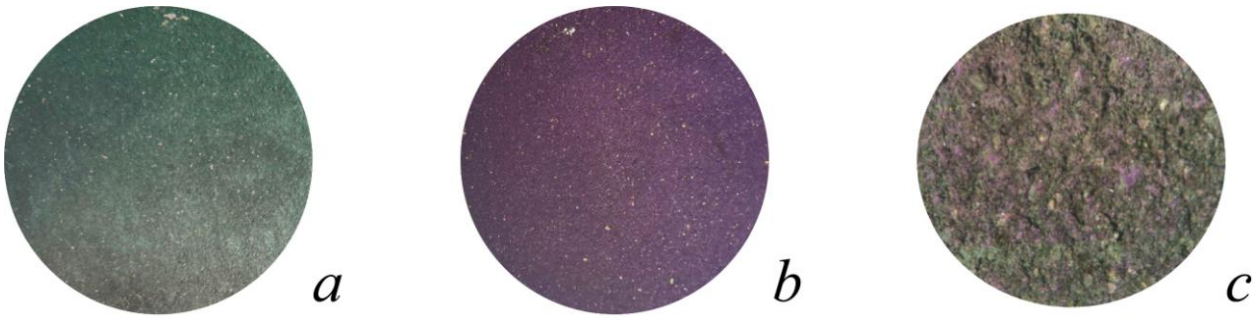

Figure S11. Color change in the powdered polycrystalline sample of **1**·0.5THF freshly prepared (*a*) and after 1 hour (*b*); the surface of the powdered polycrystalline sample of **1**·0.5CH_2Cl_2 after seven days from the start of the experiment (*c*).

7. Changes in the powder diffraction patterns during transformations

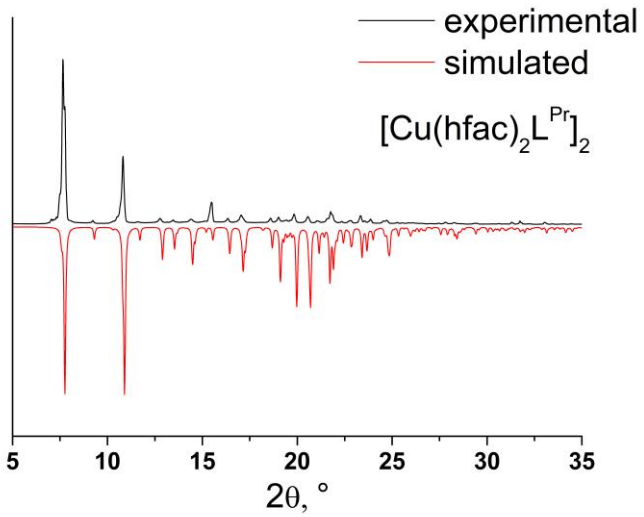

Figure S12. Theoretical and experimental diffraction patterns of $\mathbf{1}_2$.

Figure S13*a* shows the diffraction pattern of a freshly prepared powdered sample of **1**·0.5THF, demonstrating its complete correspondence to the theoretical one simulated based on the single crystal X-ray diffraction data. Over time, a gradual change in the diffraction profile was observed (Figure S13, *c*), and after one day, it completely corresponded to that of $\mathbf{1}_2$ (Figure S13, *b*).

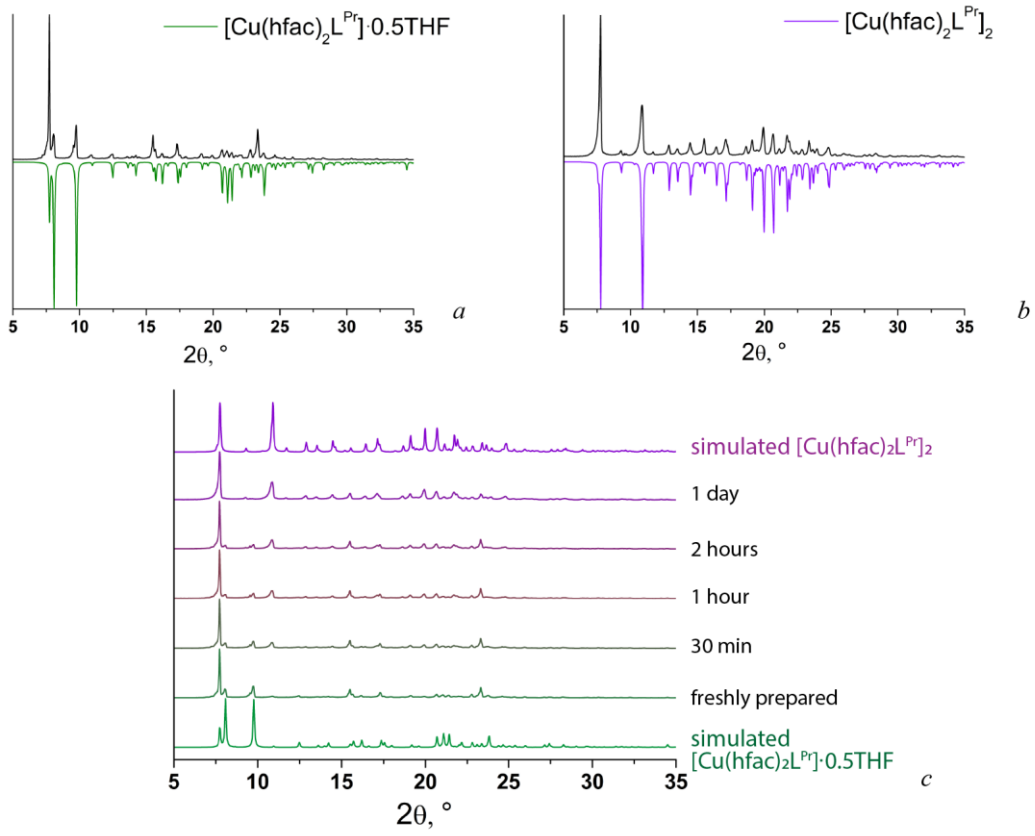

Figure S13. Diffraction patterns of **1**·0.5THF freshly prepared powder sample (*a*), diffraction patterns over time (*b*), and after one day from the start of the experiment (*c*).

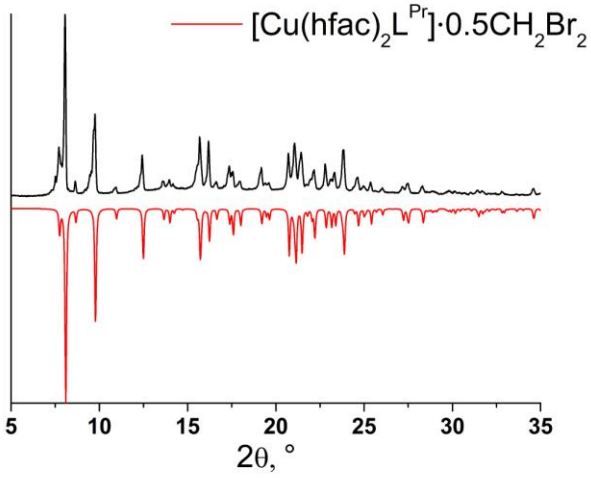

Figure S14. Full diffraction pattern of **1**·0.5CH_2Br_2 freshly prepared powder sample.

The change in the diffraction pattern for the freshly prepared sample of **1**·0.5CH_2Cl_2 over time exhibited a similar character to **1**·0.5CH_2Br_2 (Figure 6). Powder X-ray diffraction (PXRD) confirmed the purity of the initial polycrystalline sample (Figure S15, *a*). Within a day, the appearance of additional peaks in the region of ~9 and 11° was observed, corresponding to the unsolvated complex **1** (Figure S15, *b*, *c*). The near absence of peaks from $\mathbf{1}_2$ in the diffraction pattern may indicate that the proportion of

the binuclear complex is insufficient to be detected by PXRD, or due to the partial amorphization of the sample. Indeed, during the experimental procedures, the powder color remained green, but small violet crystals were formed on the surface (Figure S11, *c*), which presumably correspond to the $\mathbf{1}_2$ phase. Unfortunately, these crystals were small and had a nearly completely amorphous structure, making it impossible to determine even the parameters of their elementary cell using PXRD. Nevertheless, on a large single crystal of $\mathbf{1}\cdot 0.5CH_2Cl_2$, a solid-phase transformation to $\mathbf{1}_2$ on the crystal surface was demonstrated, as described in the article.

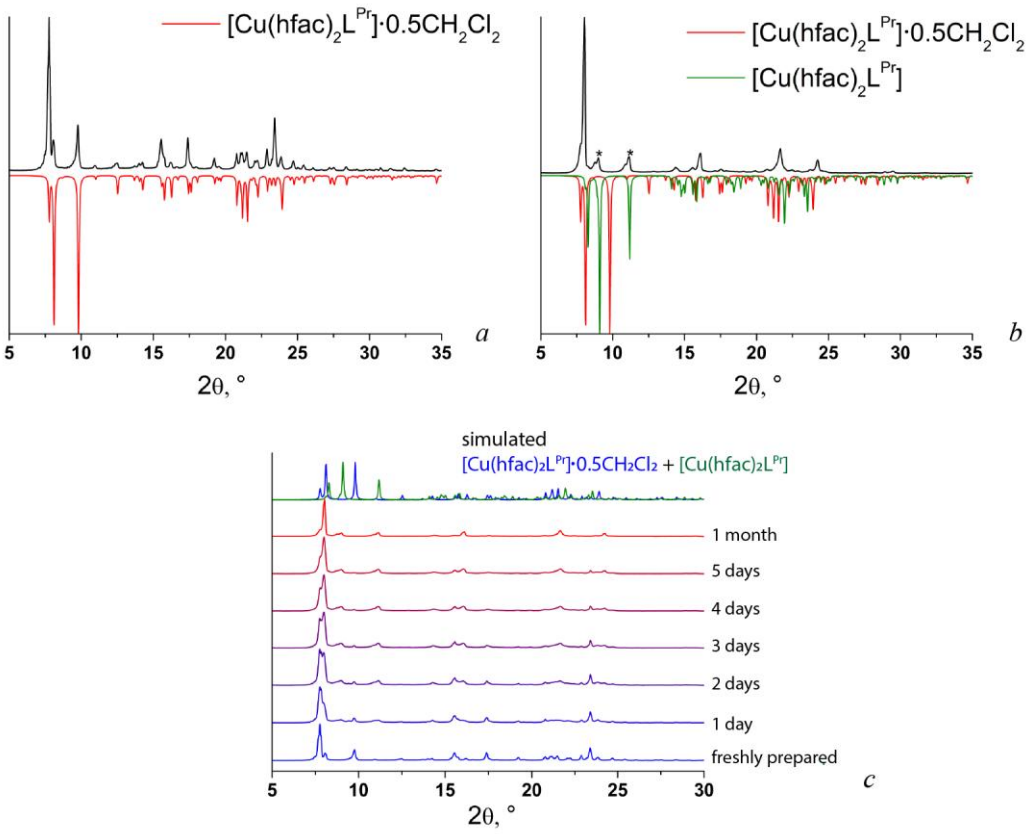

Figure S15. Diffraction patterns of $\mathbf{1}\cdot 0.5CH_2Cl_2$ freshly prepared powder sample (*a*), after one month from the start of the experiment (*b*), and diffraction patterns over time (*c*). Peaks corresponding to **1** are indicated by asterisks.

The diffraction pattern of the freshly prepared sample of $\mathbf{1}\cdot 0.5CHCl_3$ completely matches the theoretical pattern, confirming the purity of the sample (Figure S16, *a*). Weakly intense peaks in the region of ~9 and 11° (Figure S16, *c*), characteristic of the **1** phase, began to appear as early as the next day and became clearly evident after three days (Figure S16, *b*). The peak at 8.2° also corresponds to the phase of this complex.

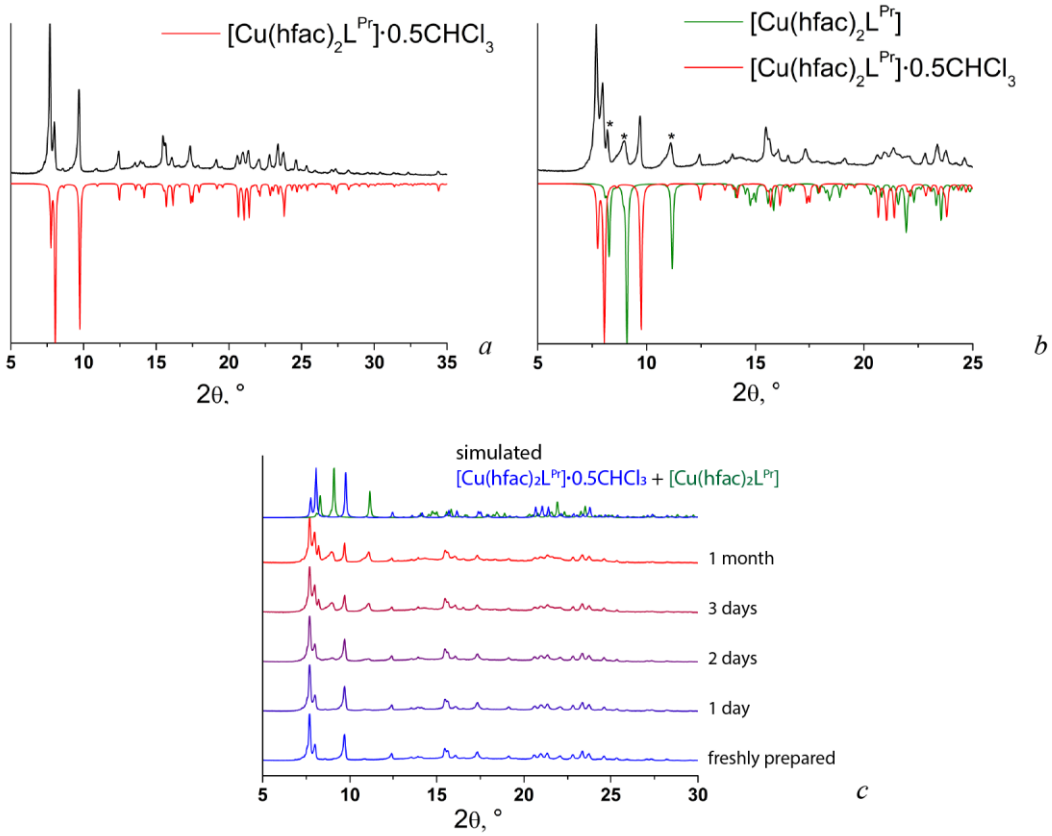

Figure S16. Diffraction patterns of **1**·0.5$CHCl_3$ freshly prepared powder sample (*a*), after three days from the start of the experiment (*b*), and diffraction patterns over time (*c*). Peaks corresponding to **1** are indicated by asterisks.

8. TG and DT analyses

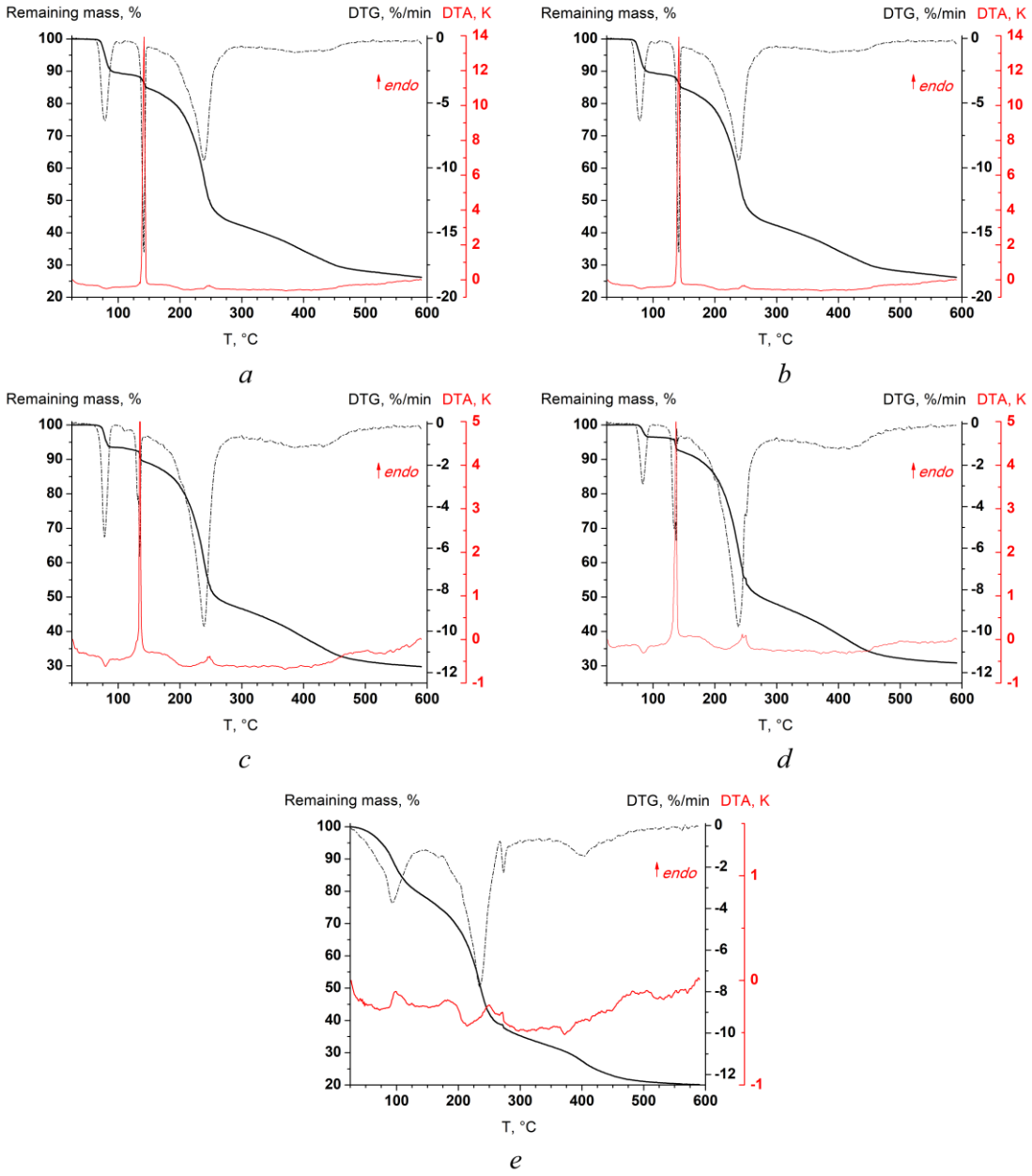

Figure S17. TG (black solid line) and DT (red solid line) analyses of **1**·0.5CH_2Br_2 (*a*), **1**·0.5CH_2Cl_2 (*b*), **1**·0.5$CHCl_3$ (*c*), **1**·0.5$(CH_3)_2CO$ (*d*) and **1**·0.5THF (*e*). The first derivative of the TG curve is represented as a black dash-dotted line. The weight loss in the range 70 – 100 °C is consistent with calculated results deduced from single crystal X-ray diffraction, i.e., ca. 0.5 solvent molecules. The decomposition point of **1**·0.5THF is close to the temperature at which all solvent molecules are lost.

9. Time-resolved IR spectroscopy

The analysis of changes in the IR spectra (recorded every 15 minutes over 20 hours) revealed a gradual alteration in line intensities (the areas with the most significant changes are highlighted in yellow on Figure S17). The nearly complete match of the last spectrum (after 20 hours) with the

spectrum of the binuclear $\mathbf{1}_2$ also confirms the PXRD data on the complete transformation of **1**·0.5THF into $\mathbf{1}_2$ within one day.

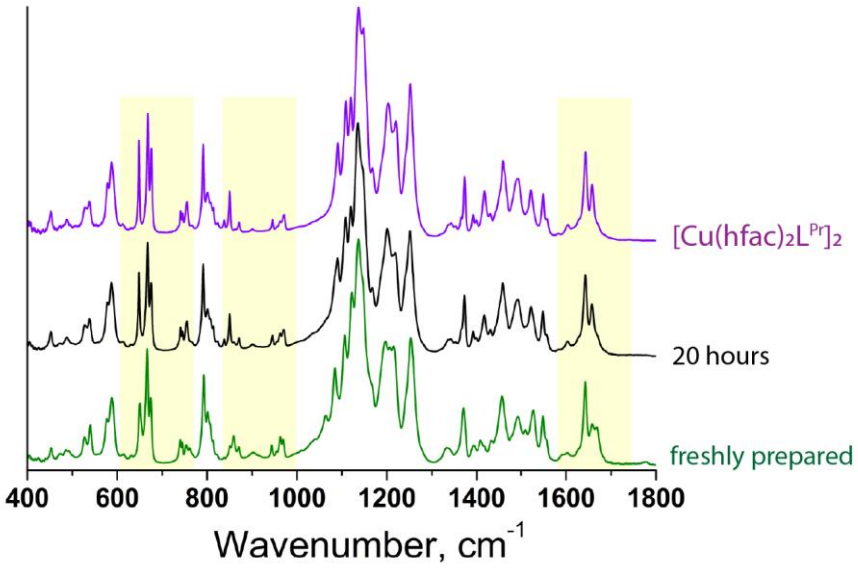

Figure S18. FTIR spectra for the freshly prepared sample of **1**·0.5THF (green), after 20 hours from the start of the experiment (black), and for $\mathbf{1}_2$ (violet).